remote sensing

MDPI

Article

Geomorphological Insights to Analyze the Kinematics of a DSGSD in Western Sicily (Southern Italy)

Chiara Cappadonia [1], Pierluigi Confuorto [2,*], Diego Di Martire [3], Domenico Calcaterra [3], Sandro Moretti [2], Edoardo Rotigliano [1] and Luigi Guerriero [3]

[1] Department of Earth and Marine Sciences (DiSTeM), University of Palermo, Via Archirafi, 22, 90123 Palermo, Italy; chiara.cappadonia@unipa.it (C.C.); edoardo.rotigliano@unipa.it (E.R.)
[2] Earth Sciences Department, University of Firenze, Via La Pira, 4, 50121 Firenze, Italy; sandro.moretti@unifi.it
[3] Department of Earth, Environmental and Resource Sciences, Federico II University of Naples, Via Vicinale Cupa Cintia, 21, 80126 Napoli, Italy; diego.dimartire@unina.it (D.D.M.); domenico.calcaterra@unina.it (D.C.); luigi.guerriero@unina.it (L.G.)
* Correspondence: pierluigi.confuorto@unifi.it; Tel.: +39-055-2757548

Abstract: Deep-Seated Gravitational Slope Deformations (DSGSDs) are common in many geological environments, and due to their common limited displacement rate, they can remain unrecognized for a long time. Among the most significant events in Sicily is the Mt. San Calogero DSGSD. To contribute to a better understanding of its characteristics, including the geologic setting promoting its development, ongoing kinematics, and mechanism, a specific analysis was completed. In this paper, the results of this analysis, based on a three-folded strategy, are provided and interpreted in the context of DSGSD predisposing conditions and controlling factors. Especially, field observations associated to visual interpretation of aerial imagery were used for the identification and mapping of main geological features and landforms, high-resolution X-Band DInSAR data enabled researchers to fully characterize the deformational behavior of the slope, while a reduced complexity slope stability analysis allowed them to reconstruct the deep geometry of the DSGSD. Results from the analysis indicate that the DSGSD of Mt. San Calogero is composed of three blocks corresponding to fault-bounded tectonic elements and characterized by a specific kinematics and sensitivity to external forcing (i.e., rainfall), multiple landslides are associated to the DSGSD in the area and the deep geometry of the DSGSD is concave upward and resemble the characteristics of a rotational slide. The interpretation of the results suggests that the formation and the deformation of the Mt. San Calogero DSGSD are linked with the local and regional fault systems related to the Sicilian orogen, while shallow landslides are triggered, in clayey terrains, mostly by rainfalls. In addition, the integrated approach reveals that active tectonics and rainfalls in the San Calogero massive relief are the main driving forces of its different deformation behavior.

Keywords: DSGSD; InSAR; slope stability; landslides; Italy

Citation: Cappadonia, C.; Confuorto, P.; Di Martire, D.; Calcaterra, D.; Moretti, S.; Rotigliano, E.; Guerriero, L. Geomorphological Insights to Analyze the Kinematics of a DSGSD in Western Sicily (Southern Italy). *Remote Sens.* **2024**, *16*, 4040. https://doi.org/10.3390/rs16214040

Academic Editors: Giulia Tessari, Benedetta Dini, Chiara Crippa and Elisa Destro

Received: 6 September 2024
Revised: 22 October 2024
Accepted: 25 October 2024
Published: 30 October 2024

1. Introduction

Deep-Seated Gravitational Slope Deformation (DSGSD) phenomena involve large mountain sectors, often characterized by high, large, and steep slopes, with extremely slow deformation [1]. The impact of Deep-Seated landslides, although not very visible and spectacular, is to be considered, especially in a mountain environment, because these phenomena may evolve into faster mass movements, trigger associated landforms and secondary local landslides and influence the hydrogeological structures thus gaining relevance even in terms of environmental hazard and risk. Identification and monitoring of these phenomena and their predisposing factors, through detailed field and remote sensing geological and geomorphological surveys are hence crucial to undertake the necessary actions to mitigate their effects on the territory [2,3]. DSGSD movements, although slow, can continue for long periods, producing large cumulative displacements [4–7]. Their

displacement rates are low, generally ranging from a few millimeters to several centimeters per year. Frequently, the development of secondary landsliding, such as rotational or planar slides, falls, topples, or flow-like movements (according to the geology and the geomorphology of the setting), commonly occurs. Displacement monitoring and assessment have generally been undertaken by using conventional geotechnical techniques, such as inclinometers, extensometers, or topographic devices, such as Global Navigation Satellite Systems. However, considering the general large extension of such phenomena, often characterized by complex movement patterns or different dynamics, point information is not always sufficient and useful to comprehend their kinematics and behavior in their entirety [8,9]. Even if the instrumental and topographic measurements are carried out on extensive networks, there are difficulties in achieving spatial and continuous information on displacement patterns [10]. In the last two decades, Synthetic Aperture Radar (SAR) interferometry demonstrates its full suitability for DSGSD monitoring, being able to measure very low displacement over large areas [11]. Additionally, potentially almost 30 years of archived data can be exploited in a certain area, being the first SAR missions deployed at the beginning of the 90s, thus representing a very valuable instrument to analyze long-lasting phenomena, such as DSGSDs. In particular, Differential Interferometry SAR (DInSAR), has proven to be an effective tool for landslide monitoring and analysis [12–18]; the first works on DSGSDs monitoring through DInSAR dates back to the early 2000s [19–21]. This technique has also bene-fitted from the increasing resolution of recent missions, such as COSMO-SkyMed (CSK) and Terrasar-X (up to 1 m), and shorter revisiting time (from 35 days of ERS and ENVISAT missions to up to six days with Sentinel-1 data). For instance, several cases of DSGSDs landslides have been studied recently with X-Band data: in [22–25] compared CSK imagery with other sources of data to analyze DSGSDs in Italy or in other countries, such as in Congo. The greater density and the better resolution of X-Band data, which may provide an enhanced state-of-the-art for the analysis of large moving areas, represent a common factor between these works.

As for the movement of DSGSDs, tectonic-induced strain along local faulting is frequently indicated as a main factor [26]. The link between stresses of tectonic alignments and DSGSDs has been theorized by several authors [27–29] when a combination between rock mass discontinuities and stress conditions are found. Active tectonics is also widely monitored through DInSAR techniques, providing a high-resolution assessment of surface deformations over long periods of observation [30]. More recently, a study by [31] used ALOS/PALSAR time series to understand the relationship between slope surface dynamics and the tectonic–geomorphic process of the active front of the Alai Range (Kyrgyzstan), hypothesizing that the active tectonics in the area are the main mechanisms for the DSGSD displacement. Western Sicily (Southern Italy) is one of the DSGSDs' richest regions, and many geomorphological analyses have been carried out since the end of the 70s [32–38]. More recently, geological and geomorphological evidence was collected by [37] to re-examine the triggering mechanisms of DSGSD phenomena in western Sicily, identify additional DSGSDs, and propose appropriate morpho-evolutionary models. In this work, an approach based on the integration of geomorphological evidence, collected in the field and through very high-resolution photo interpretation, archived CSK data from the second Italian Not-Ordinary Plan of Environmental Remote Sensing (PST-A in Italian) [39,40] and slope stability analysis has been adopted in the area of Mt. San Calogero, Palermo province, northern Sicily. Here, a recently identified DSGSD [36] is located, and a preliminary analysis was carried out by [41], which detected the effective movement of the rock spreading and the shallow deformational scenario of the foothill area was detected using Persistent Scatterers (PSs).

In this work, we deeply analyzed the whole setting, identifying three different geomorphological macro-sectors in the area from the massif to the Torto River (W to E) and three different tectonic sectors separated by tectonic alignments over Mt. San Calogero relief. All the detected sectors show changes in the velocity of deformation and thus in mechanical behavior, well detected by CSK data and by the geomorphological analysis. Compared to

previous works, where the analyses of DSGSDs were conducted mainly from a qualitative point of view, here an in-depth analysis of the kinematics and possible triggering factors has been achieved. Indeed, understanding the mechanism and anatomy of the DSGSD has been supported by a Finite Element slope stability analysis based on the strength reduction method, providing new insights into the behavior of tectonic-induced movement of large mountain sectors.

2. Materials and Methods

2.1. Geographical, Geological, and Geomorphological Setting

The Mount San Calogero Deep-seated gravitational slope deformations (DSGSDs) area (Figure 1) is located along the northern-central coastline of Sicily Island in Southern Italy [36,41].

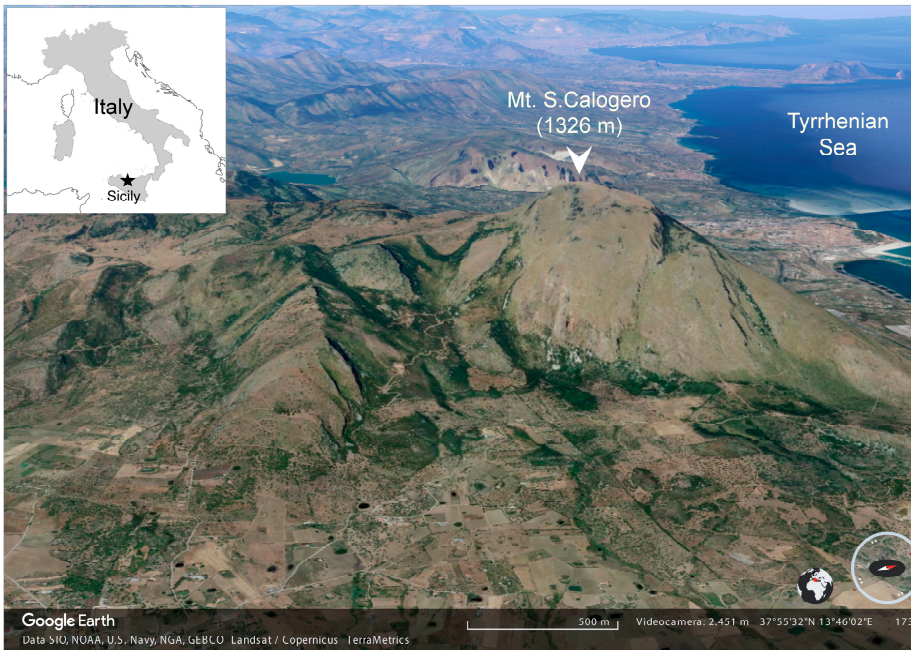

Figure 1. Satellite view of Mount San Calogero relief. In the top left inset, the location of the study area is indicated through a black star.

The topographical and geomorphological features of the study area are the result of constructive (tectonic) and destructive (erosional) forces linked to the geodynamic processes that produced a collisional system (Sicilian Fold and Thrust Belt; FTB) beside a subduction system (Figure 2b,c; [42]). These two sectors are separated by an NNW-SSE trending regional fault system with predominantly right-lateral transcurrent kinematics in the south-eastern Tyrrhenian Sea. The Sicilian FTB links the African Maghreb to the Calabrian arc and Southern Apennines and has developed in the Central Mediterranean along the plate boundary between Africa and Europe (Figure 2a). The main compressional movements started in the latest Oligocene–Early Miocene in the central southern Tyrrhenian Sea, where the counterclockwise rotation of the Corsica Sardinia and its collision with the African continental margin took place; in particular, thrusting occurred in connection with the westward subduction of the Adriatic and Ionian lithosphere beneath the Corsica–Sardinia block. Subduction and thrusting are contemporaneous with back arc-type extension in the Tyrrhenian Sea, originating high-angle extensional faults affecting the northern coastal area of Sicily and the southern Tyrrhenian Sea. The Sicilian continental subduction collisional complex appears as being formed by several tectonic and stratigraphic elements (Figure 2b). The main tectonic features are [43] the Iblean–Pelagian foreland, which is part of the African plate; the Late Pliocene–Quaternary narrow foredeep, in the footwall of the frontal sector of the thrust belt, in southern Sicily and its offshore; and the Sicilian FTB (Figure 2a).

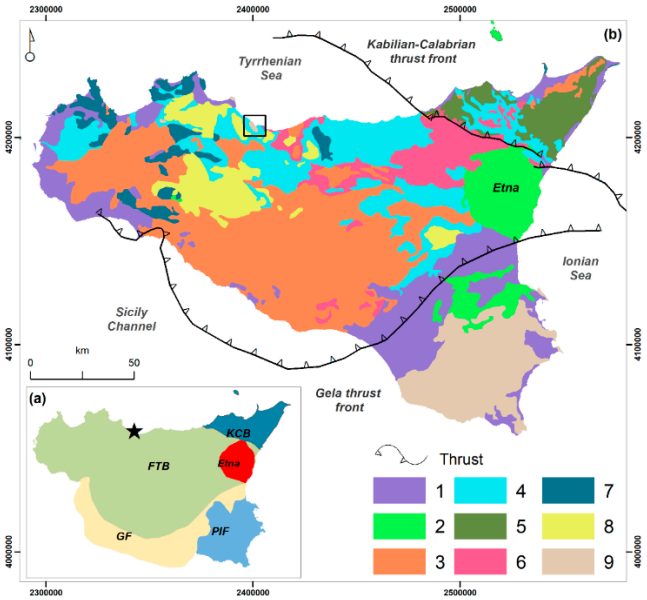

Figure 2. (**a**) Mt. Etna edifice and main elements of the collisional complex of Sicily: Kabylian–Calabrian thrust basement. The black star indicates the study area location—KCB; Fold and thrust belt—FTB; Gela foredeep—GF; Pelagian–Iblean foreland—PIF. The star indicates the study area; (**b**) Structural map of Sicily (modified from [44]): (1) Plio–Pleistocene cover, (2) volcanics, (3) upper Miocene–lower Pliocene deformed foreland deposits, (4) upper Oligocene-lower Miocene deformed foreland deposits, (5) Kabilian–Calabrian crystalline units, (6) Sicilide units, (7) Meso–Cenozoic carbonate platform deformed units (Sicilian–Maghrebian shallow-water units), (8) Meso–Cenozoic slope-to-deep-basin deformed units (Sicilian–Maghrebian deep-water units), and (9) Meso–Cenozoic carbonate platform not-deformed units (Sicilian–Maghrebian foreland).

The study area is part of the main FTB which constitutes the Sicilian orogen. The deformed substrate here consists of two main thrust wedges: one of them composes the slices of Sicilide units overthrusting the Oligo–Miocene siliciclastic successions of Numidian Flysch; the other, of Mesozoic deep-water carbonate imbricates that form mountain ranges, often characterized by the cropping out major ramp-anticlinal structures such as Mt. San Calogero. These structures show NW–SE direction and southwestward vergence [45]. In this sector, during the Middle Miocene (Serravallian)—Early Pliocene time interval, a wedge-top depositional zone developed on the underlying thrust belt to constitute an often incomplete succession of lithostratigraphic units, such as marine clays, siltstones, sandstones, continental conglomerates, and fan delta sandstones [45].

At the scale of the study area, the main structural elements are the overthrust of Meso–Cenozoic carbonate rocks over Tertiary silico–clastic deposits and the extensional and transtensional faults, which displaced and dissected the orogenic belt related to the opening of the Tyrrhenian Sea during the Plio–Quaternary [46]. The inverse high-angle faults and subsequent Pleistocenic NW–SE/NE–SW normal faults segment the whole coastal area, giving rise to a series of landforms and structures that break the physical continuity of the mountain range. The coastal sector in which the study area is marked by a coastal plain and the isolated relief of Mt. San Calogero, an exhumed homogeneous relief isolated by block faulting and stream incision and bounded by inclined structural surfaces and fault slopes. The outcropping lithotypes are Cenozoic and Mesozoic rocks, a few hundred meters thick, and previously subject to compressive stresses (mainly dolostones and dolomitized limestones in massive beds, intensely fractured and karstified (Figure 3) [47]. In this context, Mt. San Calogero is mostly formed by the Mesozoic rocks of the Crisanti formation, the Scillato formation, the Fanusi formation, and the Mufara formation. Overall, while the Crisanti and the Fanusi are primarily composed of calcareous and dolomitic breccias, locally

associated with argillites and marls, the Scillato and the Mufara formations are mostly represented by the association of calcilutites, argillites, and marls.

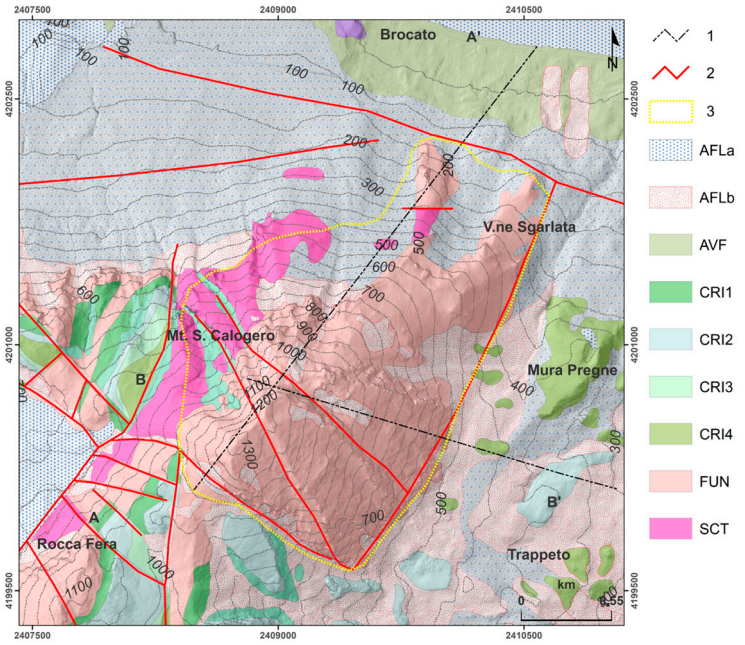

Figure 3. Geological Map of the study area (modified from [47]). Geological cross-section A–A′ and B–B′ (1); Tectonic lineaments (2); DSGSD area (3); Detritus, eluvial and colluvial deposits (AFLa); Landslides deposits (AFLb); Varicolored shales and marls, often tectonized. Cretaceous–Paleocene (AVF); Crisanti formation (CRI): Laminated radiolarites with calcilutites. Upper Toarcian–Lower Tithonian (CRI1); Calcareous breccias and conglomerates interbedded with calcarenites. Tithonian–Necomian (CRI2); Siliceous shales and marls. Hautervian–Albian (CRI3); calcareous breccias and biocalcarenites. Cenomanian–Maastrichtian (CRI4); Calcilutites alternating with marls and calcarenites. Upper Carnian–Raethian. Scillato formation (SCT); White grayish, dolomitic breccias, dolorudites, and doloarenites. Lower Liassic. Fanusi formation (FUN).

The main thrust surfaces are buried, and at the foot of the Mount, the high-angle faults create new contacts between Mesozoic successions and Cenozoic clayey terrains. The latter is covered over a wide sector by continental deposits such as detritus, eluvial, and colluvial deposits (Figure 3) This sector and the eastern side of the study area are obliterated by a wide sector of about 1.5 km^2 (MS_2) where the outcrops of continental deposits extend from the slopes for about 1.5 km until contact with the clayey outcrops which, instead, constitute the MS_3 sector. The present-day setting results from the change in stress conditions caused by the high-angle faults, which have put the brittle carbonate rocks and ductile clayey terrains into contact, thus creating displacement areas, especially in the northeastern sector of the structure, as confirmed by DInSAR data [41].

2.2. SAR Data

Archived SAR data used here belongs to the second Italian Not-Ordinary Plan of Environmental Remote Sensing (PST-A in Italian). This plan, conceived to support the administration for land management activities, had as its main objective to increase and update the previous database, implementing new COSMO-SkyMed (CSK) frames, acquired by ASI (Italian Space Agency) in the framework of the Map Italy project [48]. The CSK system is made of a constellation of four mid-sized satellites, each equipped with a high-resolution SAR sensor that operates in the X-band. A frame of 40 × 40 km was selected, covering the territories of Termini Imerese, Caccamo, and Sciara municipalities, and includes 49 images acquired over ascending orbit with an average repeat cycle of 16 days, covering the time interval 2011–2014. This data were processed through the Persistent Scatterer

Pair (PSP, [49])technique, allowing us to obtain about 340,000 Persistent Scatterers (PS) for the frame of interest, each containing information about the displacement rates at each acquisition, the average displacement value for each year of monitoring, the standard deviation of the velocity, and the coherence. The basic assumption of the PSP technique is that every PS is identified and analyzed only by working with pairs of points called arcs; for further details about the algorithm, interested readers can refer to [49].

2.3. Slope Stability Analysis

To enhance the analysis of the DSGSD at San Calogero and to understand the conditions that promote its development and long-term evolution, as well as the influence of the geological setting, a Finite Element slope stability analysis was conducted using a strength reduction method implemented in the ADONIS 3.90 software [50]. The geological section BB′ from Figure 3 was used for the analysis, and the properties of the geological materials forming Mount San Calogero were derived from technical literature, field observations, and measurements.

Given that most of the geological materials forming the slope are heterogeneous rock masses and jointed rock formations, their mechanical behavior at failure was described using a Mohr–Coulomb failure criterion, which was derived by linearizing a parameterized Hoek and Brown envelope (for a σ3max variable between 3 and 15 MPa). The failure behavior of the argillites and marls of the Mufara (MUF) formation was described using the Mohr–Coulomb criterion, parameterized based on available data for friction angle φ and cohesion c. Table 1 lists the physical and mechanical parameters assigned to the identified geological formations/members.

Table 1. Physical and mechanical parameters of geologic materials considered for the analysis. Grey cells contain Mohr–Coulomb parameters used for stability analysis. The acronym of each geological formation is reported in Figure 3.

Parameter	MUF	FUN	SCT	CRI1	CRI2	CRI3	CRI4	ISO
Unit weight (kg/m^3)	2100	2500	2500	2200	2300	2400	2500	2500
UCS (MPa)	/	90	75	40	80	50	70	/
GSI	/	60	40	30	50	30	30	/
mi	/	9	7	6	9	6	7	/
D	/	0	0	0	0	0	0	/
Young (MPa)	4000	17,000	5000	2000	9000	2300	2600	5000
Poisson	0.3	0.3	0.3	0.3	0.3	0.3	0.3	0.3
φ (°)	30	45	35	30	45	30	35	/
c (MPa)	0.5	2.5	1.2	0.6	1.3	0.8	0.65	/

For the stability analysis, a static strength reduction method was used, which accounts for the reduction of both the friction angle and cohesion during calculation. Additionally, the rocks underlying the Mufara formation were considered to exhibit elastic behavior to minimize plastic deformation at depth, which would be inconsistent with available data. This approach, starting from a theoretical pre-landslide condition represented by appropriate mechanical parameters, can estimate the deformation distribution due to potential landslide development in relation to a progressive reduction in material strength, consistent with long-term slope evolution.

Given the challenge of considering the heterogeneity of each geological formation/member and the resulting spatial variability of physical and mechanical parameters, the analysis results need to be interpreted in the context of slope evolution, focusing on the spatial distribution of deformation rather than its magnitude. Furthermore, to fully consider the influence of site conditions, major geological structures were incorporated into the

numerical model. Specifically, interfaces representing major geological structures were assigned a friction angle of 25° and normal and shear stiffness of 2×10^{10} Pa/m. The results of the stability analysis included an estimation of the pre-landslide factor of safety, considering the absence of pore-water pressure and a total displacement distribution.

3. Results

3.1. Field Activity and Geomorphological Characterization of the Area

The Mt. San Calogero is a ramp-anticlinal structure with a NW–SE direction and south–southwestward vergence. A strong tectonic disturbance occurs in the southern part as the effect of a thrust involving the Oligo–Miocene siliciclastic successions of Numidian Flysch and the syntectonic deposits (Figure 4a,b). The western side of Mt. San Calogero is bordered by a system of direct and transtensive faults with N–S and NNE–SSW directions, lowering the adjacent reliefs and juxtaposing the Mesozoic carbonate rocks with the siliciclastic Numidian successions (Figure 4b). The steeply inclined northern side of the structure is characterized by the presence of normal faults with ESE–WNW and ENE–WSW directions, which decrease in intensity towards the North (Figure 4a).

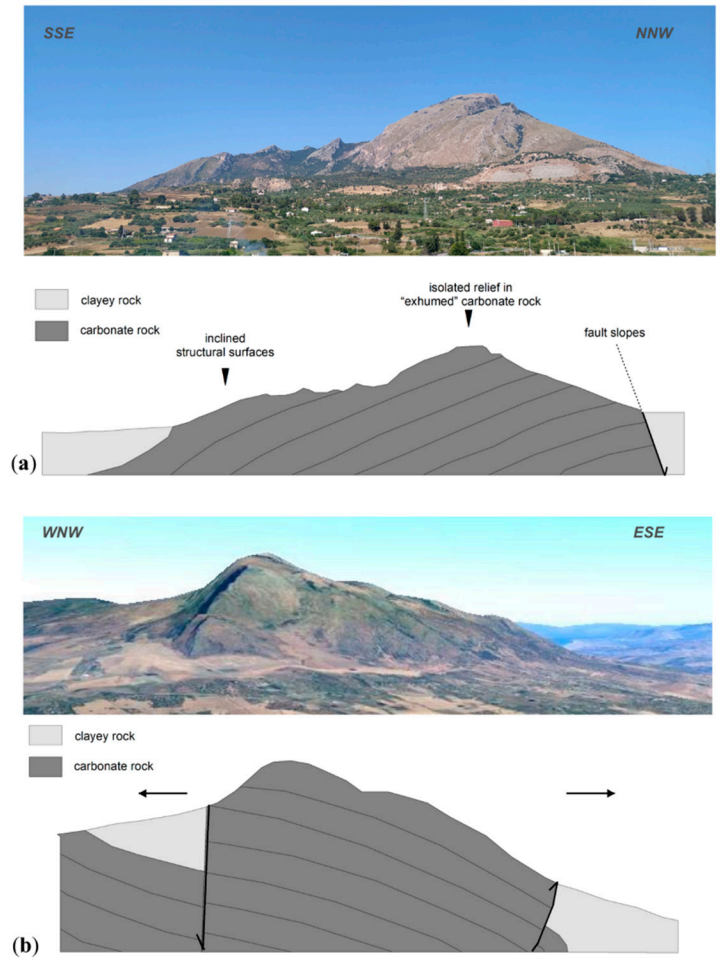

Figure 4. Schematic representation of the ramp-anticlinal structure of the S. Calogero Mount. (**a**) Panoramic view and schematic reconstruction that emphasizes the southern side interesting by a tectonic disturbance (thrust) and direct fault which affects the northern side of the structure according to [36]. (**b**) Panoramic view and schematic reconstruction according to [37] that emphasizes the strong tectonic disturbance occurs in the southern part as the effect of a thrust involving the Oligo–Miocene siliciclastic successions and the transtensive faults which juxtaposing the Mesozoic carbonate rocks with the siliciclastic Numidian successions; the black arrows indicate the tensile stress-direction.

From the geomorphological point of view, in the general area encompassed in Figure 5, it is possible to identify three different geomorphological macro-sectors named MS_1, MS_2, MS_3, and MS_4 respectively (Figures 5 and 6). Sector MS_1 coincides with the isolated, homogeneous relief in "exhumed" carbonate rock produced by differential erosion and bounded by inclined structural surfaces and fault slopes. In the uppermost part of Mt. San Calogero, typical landforms indicate the presence of DSGSDs [38], such as trenches, bulges, depression, scarps, and fractures; this morphological evidence is prominent on the northern part of the homogeneous relief of MS_1. The northern side of the sector shows up very inclined because of the effect of the normal faults with ESE–WNW and ENE–WSW directions, isolating three large blocks (B1, B2, and B3; Figures 5 and 6) according to vertical displacements characterized by steep fault scarps.

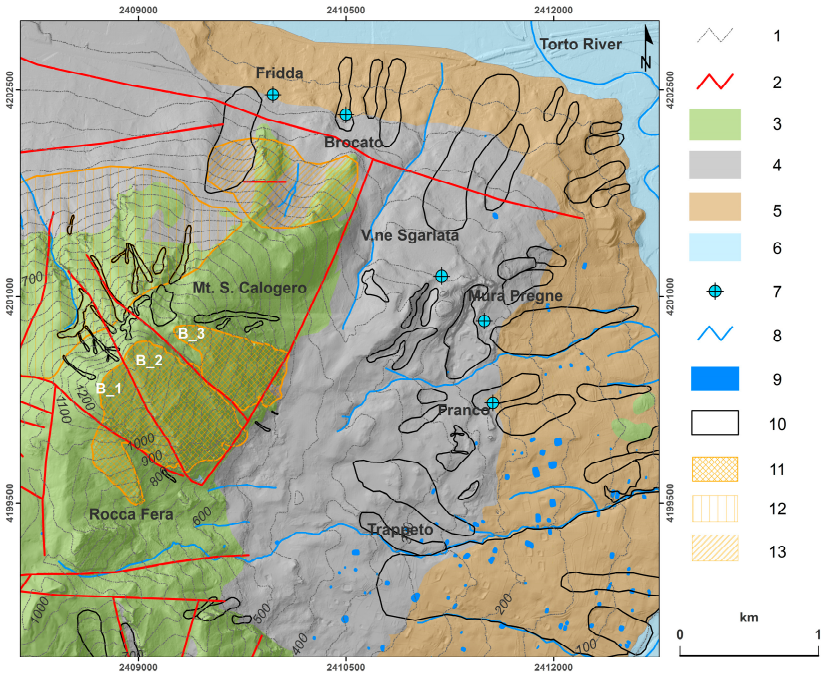

Figure 5. Geomorphological map of the study area. (1) Contour line (50 m); (2) Tectonic lineaments; (3) Geomorphological macro-sector MS_1, (4) Geomorphological macro-sector MS_2; (5) Geomorphological macro-sector MS_3; (6) Geomorphological macro-sector MS_4; (7) Spring; (8) Drainage; (9) Water body; (10) Landslide; (11) Inclined structural surface; (12) Fault line scarp; (13) Fault slope. In the map, the locations of the sub-sectors of MS_1 with the symbols B_1, B_2, and B_3 are, also, indicated.

Moreover, in the MS_1 sector, debris flow and rockfall phenomena occur at the top of the relief, the fault slope (N–W sector), and the inclined structural surface (S–E sector). On the fault slope in the northwestern part of MS_1, some large blocks, having previously slid down, protrude from the talus slope (Figure 6c). Here, rockfall phenomena occur at the marginal carbonate scarps and on a quarry front in the foothills of B3 (Figure 6b). At the base of B3, another high-angle normal fault brings the brittle rocks constituting the homogenous relief and the ductile clayey terrains into contact, influencing the general structural setting and determining the presence of contact springs (Fridda and Brocato springs in Figure 5). This sector and the eastern side of the study area are obliterated by a wide band of several km^2 (MS_2) where the outcrops of continental deposits extend from the slopes for about 1.5 km until contact with the clayey outcrops, which, instead, constitute the MS_3 sector.

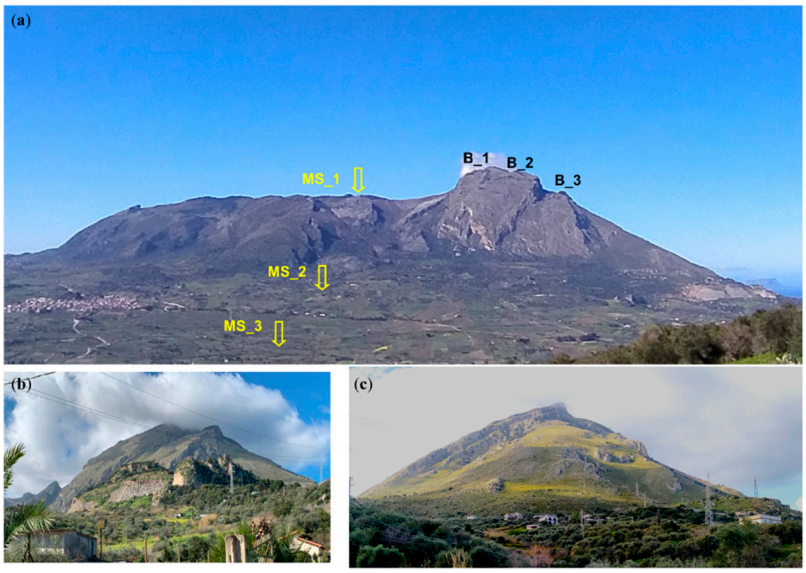

Figure 6. (**a**) Panoramic view of the study area that highlights all the geomorphological macro-sectors and the sub-sectors of MS_1; (**b**) Quarry front in the foothills of B3; (**c**) Large blocks, previously sliding down, in the northwestern part of MS_1.

In the MS_2 and MS_3, the slopes show an average gradient of 15 degrees, except for those areas in MS_2 where there are rocky masses, detached from the homogeneous relief in the past. Two archaeological sites are located here: the first, named Mura Pregne, is a place where, since the Upper Palaeolithic, human groups have settled, leaving megalithic walls and pseudo-dolmen, partially destroyed by quarry activity in the 70s; the second, the Franco rock shelter, shows prehistoric finds scattered on the surface and linear incisions on the walls of the rocky outcrop [51]. These places are also affected by several rockfall phenomena while the less inclined slopes are affected by erosion processes and surficial landslides. The MS_3 sector consists of clayey terrains on very gentle slopes and is characterized by the presence of surficial landslides and many wetlands, as also indicated in [52], which provides a new landslides inventory for the Torto River catchment area, distinguishing various typologies, such as slide, flow, and complex landslides. The natural drainage network is poorly dense due to the strong anthropization (mainly cultivated areas, secondary roads, irrigation waterways, wells for irrigation, and artificial ponds) that characterizes the lowest slopes about the MS_2 and MS_3.

The fracture networks of Mesozoic units have led to the development of a deep carbonate aquifer with important groundwater flow systems; the main groundwater flow directions are the NNE and SSE [53].

Some springs discharge along the connecting area with the MS_2 and MS_3 sectors due to the permeability contrast between the two sectors; those linked to the SSE flow direction are found in the correspondence of the two archaeological sites mentioned above; other springs, instead, following the NNE direction, are located in the northern part of the study area, in the districts of Brocato and Fridda mentioned above. The most unstable areas are situated along the connection area between the MS_2 and MS_3 but also close to the stream (Vallone Sgarlata), set on the fault line with SSE–NNW direction, which could be an effluent stream that receives or drains groundwater baseflow. A fourth area, (MS_4), was also identified; it is morphologically distinct from the other sectors coincides with the fluvial plain of the Torto River, which constitutes the northeastern physiographic limit of the study area.

3.2. SAR Analysis of the Area

The analysis of the deformation of the Mt. San Calogero area was conducted over 40,376 targets identified in the study area and derived by the application of the PSP algorithm on the set of CSK images (Figure 7). The analysis was limited, in this phase, to the slopes facing N and E of Mt. San Calogero and its foothill area, for a total of 14 km^2. The total PS density in this area is 2.884 PS/km^2, a remarkable amount even considering the scarce presence of urban artifacts in the area; in this case, the high coherence (0.75 on average) is given by the lack of vegetated cover and presence of rocky outcrops, which makes the E slope of Mt. San Calogero entirely reflective to SAR. Indeed, this slope sector reaches values of PS density of 9.900 PS/km^2, compared to the valley area, where eluvial and clay deposits are exposed and characterized by lower PS density (1.400 PS/km^2).

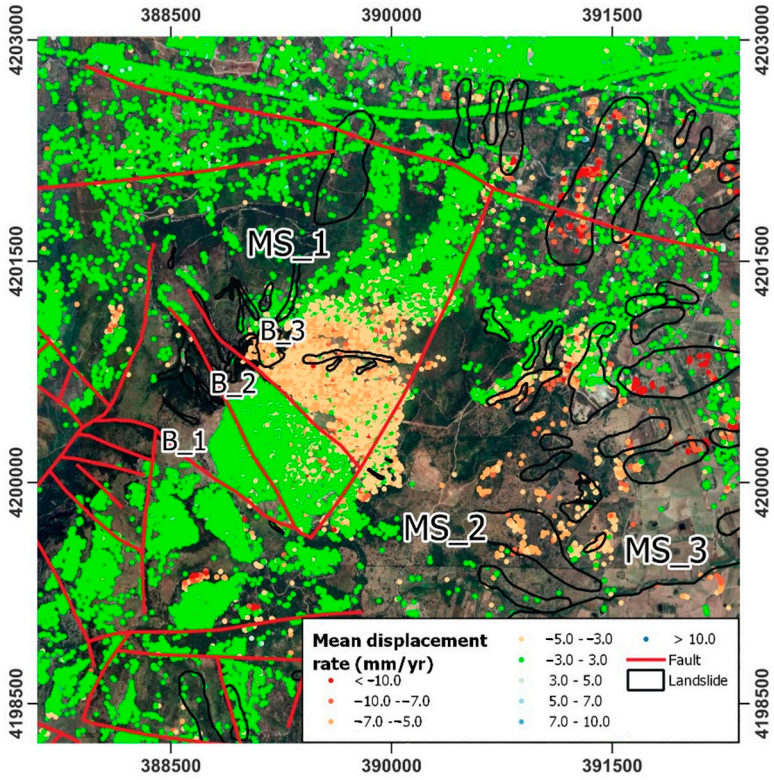

Figure 7. Average displacement map of Mt San Calogero area obtained with CSK data over ascending orbit, in the timespan 2011–2014.

Thus, the elevated concentration of PSs along the slope of Mt. San Calogero makes DInSAR analyses very suitable, permitting a detailed characterization of the DSGSD. In this case, by evaluating the PS displacement rates, three distinguished deformation patterns (B_1, B_2, and B_3) can be observed over the Mt. San Calogero relief, consistent with those identified during field activity and geomorphological characterization of the area (see Section 3.1):

- a first pattern (Block 1; B_1), in the highest part of the slope, with average values of velocity in the timespan considered of −1.3 mm/yr along the LoS (Line of Sight), with minimum and maximum velocities of −6.5 and 1.1 mm/yr, respectively.
- a second pattern (Block 2; B_2), proceeding northwestward, characterized by a higher average velocity of the PSs (−2.3 mm/yr), ranging between −13.3 and 3.6 mm/yr;
- Block 3 (B_3), down the valley of Mt. San Calogero, presents average displacement rates of −4.5 mm/yr, with minimum and maximum rates of −12.7 and 2.4 mm/yr.

Figure 8 shows an in-depth analysis of Mt. San Calogero's E slope, affected by the DSGSD: in this case, an SW–NE section has been drawn to better highlight the different behavior of the three sectors, showing the various average velocities of each area and

therefore their response to the slope movement. As visible, B1 shows a slow trend of deformation, while B2 shows a slight increase in displacement. As previously mentioned, B3 shows the highest deformation across the entire Mt. San Calogero complex, extending until the carbonate rocks are exposed. Mt. San Calogero is confined to the east by a narrow valley, dividing it from an N–S-oriented ridge.

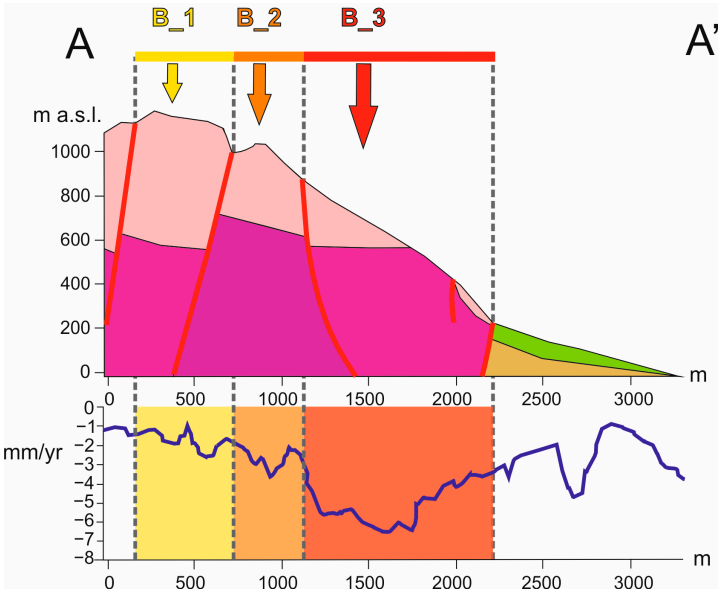

Figure 8. Top: cross-section of the Mt. San Calogero area with schematization of the three sectors. Bottom: DInSAR cross-section showing the different displacement rates of the three sectors. For the trace of cross-section (A–A′) and the colors of the geological units, refer to Figure 3. The colors of the geological cross section are referred to the colors of Figure 3, while the colors of the shaded blocks in the bottom section are, from yellow to red, referred to the displacement intensity.

The slope of such ridge, characterized by a massive presence of eluvial–colluvial materials, is also affected by shallow slope movements. In detail, PSs are spread across the entire slope sector, although with lower PS density (1.150 PS/km^2), allowing identification of four landslides, among those identified during the geomorphological mapping. The first landslide, facing north, shows average velocities of displacement, in the timespan considered, of −6.5 mm/yr, with a minimum of −24.5 mm/yr; moving southwards, another landslide phenomenon, with PS average displacement rate of −5.2 and a minimum of −10.6 mm/yr, is recorded. Finally, at the southern edge of the study area, two phenomena are encompassed, with average velocities of −4.9 and −2.2 mm/yr, and minimum peaks of −9.2 and −6 mm/yr, respectively. According to the PS map, the foothills sector also presents a distribution of several landslide phenomena. In the northern sector, four slides, identified during the geomorphological mapping, have PS average velocities of −5 mm/yr, reaching velocities of −23.6 mm/yr. Hence, a flow-like movement of 0.25 km^2 shows very high average displacement rates of −9.4 mm/yr, with the lowest rate of −42.5 mm/yr. It is worth reminding that all these deformations detected with negative values are by an eastward movement.

The cross-section of Figure 9 clearly shows the different behavior in terms of deformation between the two macro-sectors: MS_1, related to the homogeneous relief made of carbonate rock, assumes a slow-moving behavior, with rates of about 2–3 mm/yr; in contrast, the transition between MS_2 and MS_3 reveals a completely different displacement pattern, with values between 35 and 40 mm/yr.

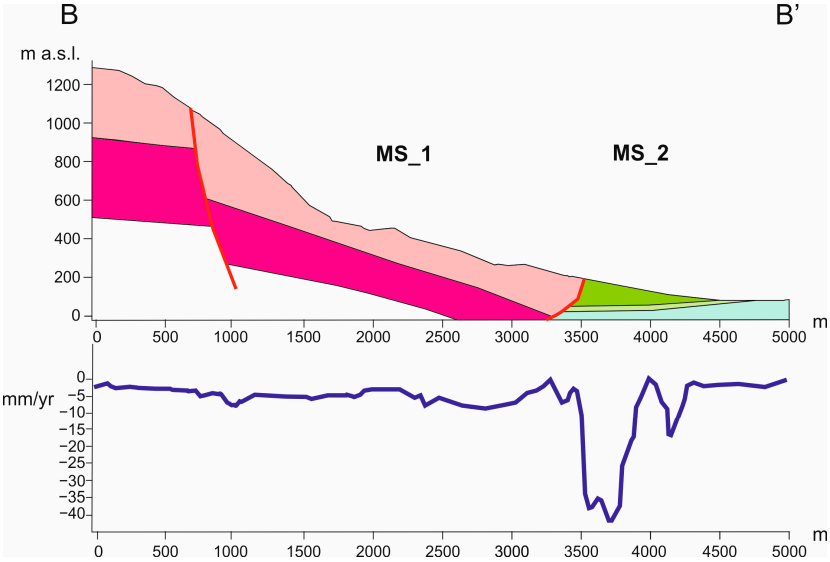

Figure 9. Cross-section of the Mt. San Calogero east flank on the top; on the bottom, DInSAR cross section showing the cumulative displacement values. For the trace of cross-section (B–B′) and the colors of the geological units, refer to Figure 3.The colors of the geological cross section are referred to the colors of Figure 3.

3.3. Slope Stability Analysis of the DSGSD

Figure 10 illustrates the numerical engineering–geological model used for the Finite Element slope stability analysis. This model includes the constitutive models that represent the mechanical behavior of the rocks forming Mount San Calogero, the boundary conditions, and the reconstructed 3-node triangular mesh with a maximum edge length of 50 m. The orange lines denote Coulomb interfaces, which represent the main faults identified in the field. These faults could affect slope stability conditions, as well as the shape, displacement, and strain distribution of the landslide.

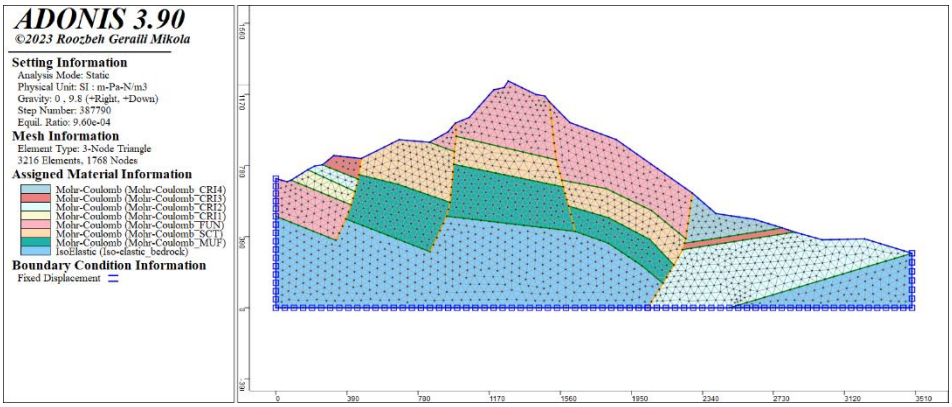

Figure 10. Numerical engineering–geological model of the slope affected by the DSGSD and considered for the analysis.

Figure 11 presents the results of the strength reduction analysis, showing the displacement distribution corresponding to a Factor of Safety estimated at approximately 2.1. As depicted in the figure, the DSGSD is anticipated to affect the eastern slope of Mount San Calogero. Higher cumulative displacement values are expected in the middle and lower sections of this slope, ranging from about 500 to 1000 m above sea level. This potentially highly active zone is bounded upslope by the upper and east-trending normal fault that cuts through the slope and extends downslope to the area where the rocks of the Crisanti

(CRI4) formations are exposed. The blue area indicates no significant displacement on the opposite slope.

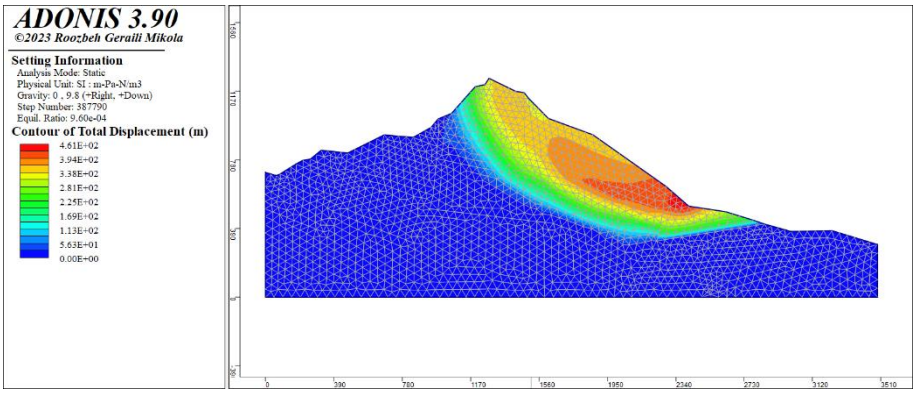

Figure 11. Displacement distribution as predicted by strength reduction slope stability analysis.

Figure 12 presents the results of the strength reduction analysis, showing the shear strain distribution in relation to the displacement distribution predicted by the method. As indicated in the figure, shear strain is distributed in a band approximately 100 m thick at the base of the slope sector affected by the DSGSD. This forms a sub-circular, concave upward zone of distributed strain, suggesting the presence of either multiple basal sliding surfaces or a damage zone. Based on the strain distribution, the maximum thickness of the DSGSD is estimated to be around 500 m. Strain diffusion is observed at the upper fault bounding the highly active zone of the slope. Additionally, strain concentration is predicted within the Crisanti (CRI3) formation, likely due to its relative weakness compared to surrounding rocks. Overall, the displacement and strain distribution in the numerical model suggest a rotational sliding mechanism for the DSGSD landslide, with strain distributed within a significantly thick band.

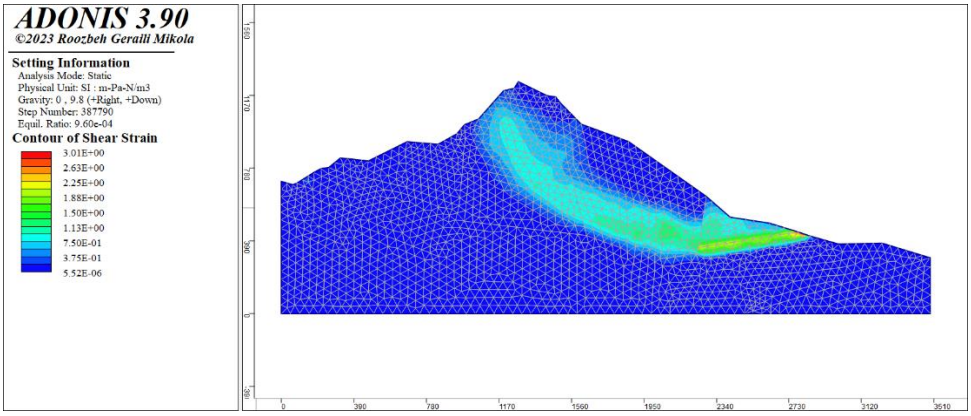

Figure 12. Strain distribution as predicted by strength reduction slope stability analysis.

4. Discussion

In this paper, an in-depth study of one of the most important DSGSDs of Western Sicily [36] is provided through a three-folded strategy: on one hand, the identification and mapping of main geological features and landforms, performed through field activities and photo-interpretation, provided an updated inventory of the displacement phenomena; on the other hand, the use of very high-resolution DInSAR data has enabled the possibility to fully characterize the different deformational behaviors among the three blocks composing the mountain massif of the Mt. San Calogero and within the three macro-sectors formed by different lithologies; finally, the use of a reduced complexity and strength reduction-

based slope stability analysis allowed us to derive data about a potential deep geometry of the DSGSD.

The field activities were fundamental in observing and interpreting the main landforms and the triggering cause of the DSGSD of San Calogero relief. The primary trigger for the DSGSD, here, is linked to the presence of high relief energy associated with lateral decompression of the brittle carbonate rock mass, involving ductile substratum affected by deformation, as also indicated by [36] and well documented in [54]. The local morphological setting is also a consequence of the Quaternary morphotectonic evolution, which is influenced by both block faulting in the northern coastal areas and by down-cutting across all of western Sicily [37]. Movements mostly assumed as lateral spreading, involving the carbonate relief blocks of Mt. San Calogero, originated by extensional and transpressional movements linked to the opening of the Tyrrhenian Sea [43]. The displacement behavior is typical of block-like mountain structures, as also evidenced in [55], where the progressive lowering of each block occurs from the top to the bottom. The different distribution of displacement rates shown in Figure 8 is due to the presence of different movement constraints between the sectors. Indeed, the constraints are greater in sector B_1 and lesser in sector B_3, the latter being bordered by a high-angle fault that puts the sector in contact with the clay. Such kinematics have been found in other DSGSD case studies in different geological contexts [55,56].

The usage of DInSAR data, especially when generated through the implementation of X-Band imagery such as COSMO-SkyMed data, is a key factor in verifying field observations and fully characterizing ongoing deformations, both spatially and temporally, across the whole sector. In this sense, adoption time series displacement data is a significant means of analyzing the evolution of the movements and the triggering factors.

The deformation trend evidenced either by X-Band SAR data (between 2011 and 2014) and field surveys is even confirmed by Sentinel-1 data from the European Ground Motion Service (EGMS, [57]). Indeed, such data, available on a dedicated platform (https://egms.land.copernicus.eu/ accessed on 18 September 2024), show analogous deformation in the timespan 2015–2020, especially in the ascending data (Figure 13a,b): B_1 shows an average displacement rate of −0.1 mm/yr and a minimum of −5.9 mm/yr; B_2 is characterized by average and minimum deformation rates of −1.7 and 3.6 mm/yr; and B_3 has mean and minimum rates of displacement of −2.6 and 5.7 mm/yr. The EGMS also provides information reprojected along the vertical and EW horizontal directions (Figure 13c,d). For the three blocks of the Mt. San Calogero, the main component is vertical, especially in sector B_3, with a subsiding deformation rate up to 5 mm/yr, while the horizontal one can be considered negligible.

Of concern, the homogenous relief, B3, is showing the highest deformation of the entire Mt. San Calogero complex; here, a normal high-angle fault brings the brittle rocks and the ductile clayey terrains into contact, and two other faults, parallel to this one and with prevailing vertical components, displace the blocks further upstream.

On the other hand, the shallow landslides of MS_2 show a predominant horizontal deformation eastward, confirming the different origins and triggers of these deformational patterns.

The particular structural geological setting also implies the development of a deep carbonate aquifer with important groundwater flow systems, which influence the geomorphological behavior in correspondence with the spring areas, including some of the surficial landslides characterizing the MS_2 and MS_3 sectors.

As reckoned by many authors, slow-moving DSGSDs can be reactivated or accelerated by many environmental factors, including temperature variations [8,58], which influence the precipitations, solar radiance, water circulation, and groundwater changes.

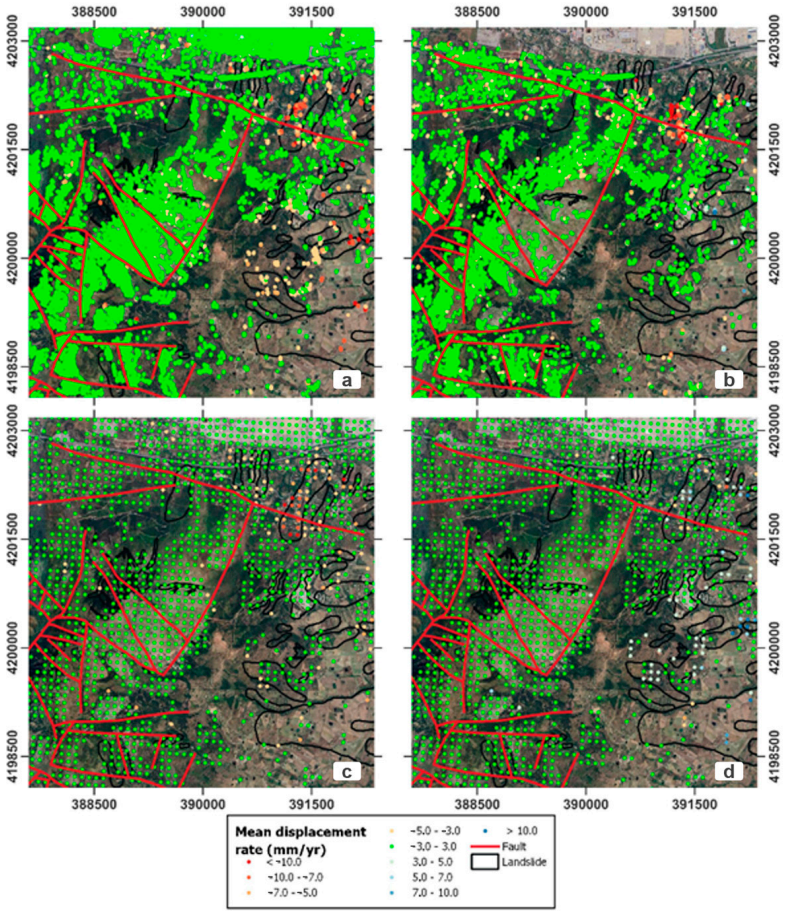

Figure 13. Deformation rate maps obtained with EGMS data: (**a**) Ascending dataset; (**b**) Descending dataset; (**c**) Vertical deformation; (**d**) Horizontal E–W deformation. Red lines represent the faults, and the black polygons represent the landslides in the Mt. San Calogero area.

For this reason, in this paper, considering the main geomorphological, hydrogeological, and hydrological features, pluviometric data were analyzed and correlated with displacement data.

For Mt. San Calogero, time series of displacement, covering the entire timespan (2011–2014) were compared to rainfall data collected in Termini Imerese station, located 11 km from the study area. Points selected belong to each one of the MSs as identified in the field activities, while rainfall data displayed in Figure 14 are summed monthly. Regarding MS_1, both the PSs considered are located over the third block of the Mt. San Calogero DSGSD; in this case, the two targets do not show any link between the temporal evolution of the displacement and rainfall peaks. Instead, a general deformation, up to about 20 mm, is observed, with a seasonal trend, with accelerations during autumns/winters and a rebound during springs/summers. MS_2, corresponding to the continental deposits, shows a different deformation pattern, as visible in Figure 7; the two points selected over one of the landslides involving colluvial material highlight a cumulative displacement of about 40 mm and a certain reaction to the precipitation peak of March 2013. Finally, MS_3 shows a further deformational scenario in the two targets selected in the WE slow flow: in this case, cumulative displacement over the three years is about 120 mm, with an immediate response to the rainy periods, as seen during February 2012 (with 167 mm of precipitations) and especially after March 2013 (187 mm), where a strong acceleration is registered, showing a cumulative displacement of 60 mm over 8 months (March–November 2013).

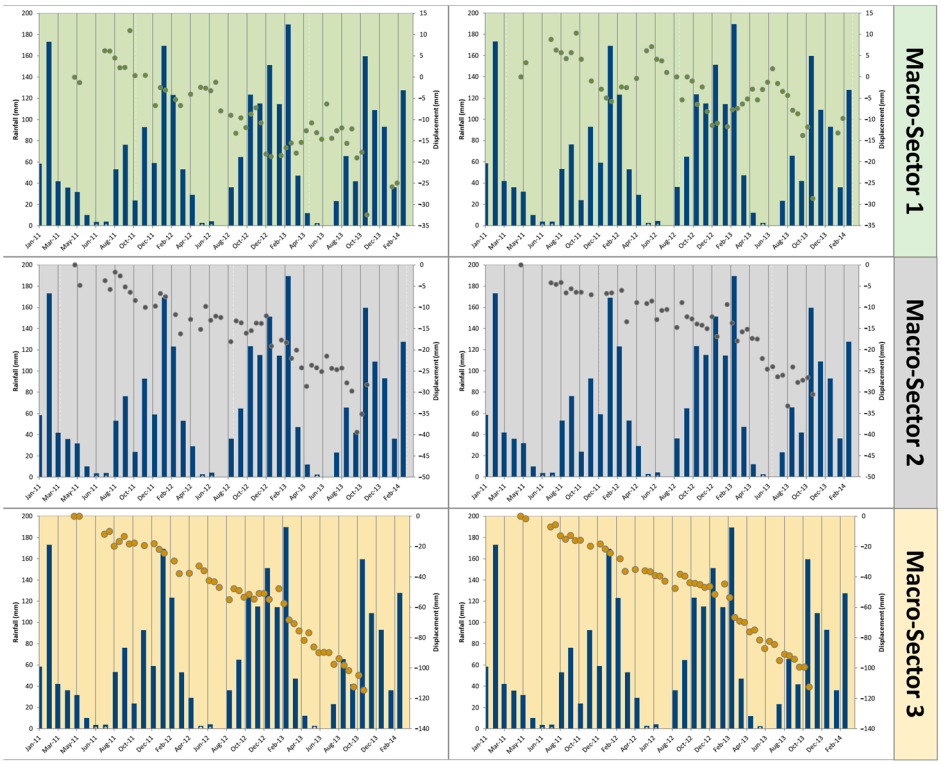

Figure 14. Time series of a couple of PSs for each Macro-Sector of Mt. San Calogero. Each time series is coupled with rainfall data available from the Termini Imerese station.

The analysis of the driving forces of DSGSDs is therefore essential, even considering their present-day low activity [51], in supporting the engineering geological activities to reduce risks, as low displacement rates may still impact elements at risk [59,60]. Additionally, DSGSD activity may represent a trigger for the development of large rockslides, posing significant risks, especially in inhabited areas.

The strength reduction slope stability analysis, executed using available data to represent the geologic setting of the slope and variability of rock properties, indicates a landslide anatomy consistent with that interpreted based on field observation and PS data. This confirms that the geological complexity of the sector of the slope effectively influence deep-seated landslide and DSGSD development. The presence of the normal fault bounding the zone characterized by higher displacement and the geologic setting of the Crisanti formation, cropping out at the landslide base, can have a significant influence on slope stability. Considering the properties of rocks forming the mount, the damage zone of the DSGSD might consist of ductile materials that can drive the observed long-term and approximately constant-rate displacement, meaning that failure might only occur after prolonged slow movement or in presence of a significant change in boundary conditions due to an extreme meteorological event or an earthquake [61].

5. Conclusions

The study shows the integration of geomorphological and tectonic insights along with Synthetic Aperture Radar Interferometry (InSAR) results to characterize and analyze the Deep-Seated Gravitational Slope Deformation of Mt. San Calogero (Termini Imerese, Palermo province, Northern Sicily) and its surrounding area. The formation and the deformation of the Mt. San Calogero DSGSD are linked with the local and regional fault systems related to the Sicilian orogen, while shallow landslides are triggered in clayey terrains, mostly by rainfalls. Regarding geomorphological evidence, three blocks can be identified in Mt. San Calogero area, separated by parallel NW–SE faults and characterized by typical landforms such as rockfalls, boulders, and secondary jointing.

COSMO-SkyMed InSAR data (2011–2014) demonstrated the different kinematics of each block, with different displacement rates (from B_1, with average velocity of −1.3 mm/yr, to B_3, with a displacement rate of −4.5 mm/yr); furthermore, the recent European Ground Motion Service Sentinel-1 data revealed the predominant vertical motion, in accordance with fault activity. Along with the DSGSD activity, shallow landslides were identified through geomorphological field activities, highlighting gentler slopes, clayey mobilized terrains, and natural water springs, while InSAR displayed intense deformation activity, up to 20 mm/yr, linked to the precipitation in the area; also in this case, the new EGMS data revealed a predominant horizontal component of the movement, in accordance with field evidence and the natural configuration of the slope. Therefore, the integrated approach combining geomorphological evidence and InSAR reveals that active tectonics and rainfall in the San Calogero massive relief are the main driving forces of different deformation behaviors. The Finite Element slope stability analysis, based on the strength reduction method, suggests an overall concave upward geometry of the DSGSD and an associated rotational sliding mechanism with strain distributed within a significantly thick band.

Author Contributions: Conceptualization, C.C., D.D.M. and P.C.; methodology, C.C., D.D.M., P.C. and L.G.; software, L.G.; investigation, C.C., D.D.M. and P.C.; data curation, C.C., D.D.M., P.C. and L.G.; writing—original draft preparation, C.C., D.D.M. and P.C.; writing—review and editing, C.C., D.D.M., P.C., D.C., L.G., S.M. and E.R.; visualization, C.C., D.D.M., P.C. and L.G.; supervision, D.C., S.M. and E.R.; project administration, D.C., S.M. and E.R.; funding acquisition, D.C., S.M. and E.R. All authors have read and agreed to the published version of the manuscript.

Funding: This research received no external funding.

Data Availability Statement: The datasets used and/or analysed during the current study are available from the corresponding author on reasonable request.

Acknowledgments: The publication was made by a researcher with a research contract co-funded by the European Union—PON Research and Innovation 2014–2020 in accordance with Article 24, paragraph 3a), of Law No. 240 of 30 December 2010, as amended and Ministerial Decree No. 1062 of 10 August 2021.

Conflicts of Interest: The authors declare no conflicts of interest.

References

1. Hungr, O.; Leroueil, S.; Picarelli, L. The Varnes Classification of Landslide Types, an Update. *Landslides* **2014**, *11*, 167–194. [CrossRef]
2. Agliardi, F.; Crosta, G.B.; Frattini, P. Slow Rock-Slope Deformation. In *Landslides*; Clague, J.J., Stead, D., Eds.; Cambridge University Press: Cambridge, UK, 2012; pp. 207–221, ISBN 978-0-511-74036-7.
3. Discenza, M.E.; Esposito, C.; Komatsu, G.; Miccadei, E. Large-Scale and Deep-Seated Gravitational Slope Deformations on Mars: A Review. *Geosciences* **2021**, *11*, 174. [CrossRef]
4. Bigotcormier, F.; Braucher, R.; Bourles, D.; Guglielmi, Y.; Dubar, M.; Stephan, J. Chronological Constraints on Processes Leading to Large Active Landslides. *Earth Planet. Sci. Lett.* **2005**, *235*, 141–150. [CrossRef]
5. Cruden, D.M.; Hu, X.Q. Exhaustion and Steady State Models for Predicting Landslide Hazards in the Canadian Rocky Mountains. *Geomorphology* **1993**, *8*, 279–285. [CrossRef]
6. Hippolyte, J.-C.; Bergerat, F.; Gordon, M.B.; Bellier, O.; Espurt, N. Keys and Pitfalls in Mesoscale Fault Analysis and Paleostress Reconstructions, the Use of Angelier's Methods. *Tectonophysics* **2012**, *581*, 144–162. [CrossRef]
7. Hippolyte, J.-C.; Bourlès, D.; Braucher, R.; Carcaillet, J.; Léanni, L.; Arnold, M.; Aumaitre, G. Cosmogenic 10Be Dating of a Sackung and Its Faulted Rock Glaciers, in the Alps of Savoy (France). *Geomorphology* **2009**, *108*, 312–320. [CrossRef]
8. Barla, G.; Antolini, F.; Barla, M.; Mensi, E.; Piovano, G. Monitoring of the Beauregard Landslide (Aosta Valley, Italy) Using Advanced and Conventional Techniques. *Eng. Geol.* **2010**, *116*, 218–235. [CrossRef]
9. Di Luzio, E.; Discenza, M.E.; Di Martire, D.; Putignano, M.L.; Minnillo, M.; Esposito, C.; Scarascia Mugnozza, G. Investigation of the Luco Dei Marsi DSGSD Revealing the First Evidence of a Basal Shear Zone in the Central Apennine Belt (Italy). *Geomorphology* **2022**, *408*, 108249. [CrossRef]
10. Tarchi, D.; Casagli, N.; Fanti, R.; Leva, D.D.; Luzi, G.; Pasuto, A.; Pieraccini, M.; Silvano, S. Landslide Monitoring by Using Ground-Based SAR Interferometry: An Example of Application to the Tessina Landslide in Italy. *Eng. Geol.* **2003**, *68*, 15–30. [CrossRef]

11. Discenza, M.; Di Luzio, E.; Martino, S.; Minnillo, M.; Esposito, C. Role of Inherited Tectonic Structures on Gravity-Induced Slope Deformations: Inference from Numerical Modeling on the Luco Dei Marsi DSGSD (Central Apennines). *Appl. Sci.* **2023**, *13*, 4417. [CrossRef]
12. Bovenga, F.; Pasquariello, G.; Pellicani, R.; Refice, A.; Spilotro, G. Landslide Monitoring for Risk Mitigation by Using Corner Reflector and Satellite SAR Interferometry: The Large Landslide of Carlantino (Italy). *Catena* **2017**, *151*, 49–62. [CrossRef]
13. Bozzano, F.; Carabella, C.; De Pari, P.; Discenza, M.E.; Fantucci, R.; Mazzanti, P.; Miccadei, E.; Rocca, A.; Romano, S.; Sciarra, N. Geological and Geomorphological Analysis of a Complex Landslides System: The Case of San Martino Sulla Marruccina (Abruzzo, Central Italy). *J. Maps* **2020**, *16*, 126–136. [CrossRef]
14. Confuorto, P.; Di Martire, D.; Infante, D.; Novellino, A.; Papa, R.; Calcaterra, D.; Ramondini, M. Monitoring of Remedial Works Performance on Landslide-Affected Areas Through Ground- and Satellite-Based Techniques. *Catena* **2019**, *178*, 77–89. [CrossRef]
15. Dong, J.; Zhang, L.; Tang, M.; Liao, M.; Xu, Q.; Gong, J.; Ao, M. Mapping Landslide Surface Displacements with Time Series SAR Interferometry by Combining Persistent and Distributed Scatterers: A Case Study of Jiaju Landslide in Danba, China. *Remote Sens. Environ.* **2018**, *205*, 180–198. [CrossRef]
16. Raspini, F.; Bianchini, S.; Ciampalini, A.; Del Soldato, M.; Montalti, R.; Solari, L.; Tofani, V.; Casagli, N. Persistent Scatterers Continuous Streaming for Landslide Monitoring and Mapping: The Case of the Tuscany Region (Italy). *Landslides* **2019**, *16*, 2033–2044. [CrossRef]
17. Solari, L.; Del Soldato, M.; Raspini, F.; Barra, A.; Bianchini, S.; Confuorto, P.; Casagli, N.; Crosetto, M. Review of Satellite Interferometry for Landslide Detection in Italy. *Remote Sens.* **2020**, *12*, 1351. [CrossRef]
18. Zhao, Q.; Lei, Y.; Ma, G.; Pepe, A.; Reale, D.; Kubanek, J.; Liu, M.; Yang, T. Surface Deformation of the Shanghai Coastal Area Revealed by a Multi-Satellite Dinsar Investigation. In Proceedings of the IGARSS 2018—2018 IEEE International Geoscience and Remote Sensing Symposium, Valencia, Spain, 22–27 July 2018; IEEE: New York, NY, USA; pp. 537–540.
19. Ambrosi, C.; Crosta, G.B. Large Sackung along Major Tectonic Features in the Central Italian Alps. *Eng. Geol.* **2006**, *83*, 183–200. [CrossRef]
20. Strozzi, T.; Farina, P.; Corsini, A.; Ambrosi, C.; Thüring, M.; Zilger, J.; Wiesmann, A.; Wegmüller, U.; Werner, C. Survey and Monitoring of Landslide Displacements by Means of L-Band Satellite SAR Interferometry. *Landslides* **2005**, *2*, 193–201. [CrossRef]
21. Saroli, M.; Stramondo, S.; Moro, M.; Doumaz, F. Movements Detection of Deep Seated Gravitational Slope Deformations by Means of InSAR Data and Photogeological Interpretation: Northern Sicily Case Study. *Terra Nova* **2005**, *17*, 35–43. [CrossRef]
22. Bayer, B.; Simoni, A.; Schmidt, D.; Bertello, L. Using Advanced InSAR Techniques to Monitor Landslide Deformations Induced by Tunneling in the Northern Apennines, Italy. *Eng. Geol.* **2017**, *226*, 20–32. [CrossRef]
23. Bordoni, M.; Bonì, R.; Colombo, A.; Lanteri, L.; Meisina, C. A Methodology for Ground Motion Area Detection (GMA-D) Using A-DInSAR Time Series in Landslide Investigations. *Catena* **2018**, *163*, 89–110. [CrossRef]
24. Samsonov, S.; Dille, A.; Dewitte, O.; Kervyn, F.; d'Oreye, N. Satellite Interferometry for Mapping Surface Deformation Time Series in One, Two and Three Dimensions: A New Method Illustrated on a Slow-Moving Landslide. *Eng. Geol.* **2020**, *266*, 105471. [CrossRef]
25. Guerriero, L.; Prinzi, E.P.; Calcaterra, D.; Ciarcia, S.; Di Martire, D.; Guadagno, F.M.; Ruzza, G.; Revellino, P. Kinematics and Geologic Control of the Deep-Seated Landslide Affecting the Historic Center of Buonalbergo, Southern Italy. *Geomorphology* **2021**, *394*, 107961. [CrossRef]
26. Agliardi, F.; Crosta, G.B.; Zanchi, A.; Ravazzi, C. Onset and Timing of Deep-Seated Gravitational Slope Deformations in the Eastern Alps, Italy. *Geomorphology* **2009**, *103*, 113–129. [CrossRef]
27. Bovis, M.J.; Evans, S.G. Extensive Deformations of Rock Slopes in Southern Coast Mountains, Southwest British Columbia, Canada. *Eng. Geol.* **1996**, *44*, 163–182. [CrossRef]
28. Dramis, F.; Sorriso-Valvo, M. Deep-Seated Gravitational Slope Deformations, Related Landslides and Tectonics. *Eng. Geol.* **1994**, *38*, 231–243. [CrossRef]
29. Ghirotti, M.; Martin, S.; Genevois, R. The Celentino Deep-Seated Gravitational Slope Deformation (DSGSD): Structural and Geomechanical Analyses (Peio Valley, NE Italy). *SP* **2011**, *351*, 235–251. [CrossRef]
30. Massironi, M.; Zampieri, D.; Bianchi, M.; Schiavo, A.; Franceschini, A. Use of PSInSAR^{TM} Data to Infer Active Tectonics: Clues on the Differential Uplift across the Giudicarie Belt (Central-Eastern Alps, Italy). *Tectonophysics* **2009**, *476*, 297–303. [CrossRef]
31. Teshebaeva, K.; Echtler, H.; Bookhagen, B.; Strecker, M. Deep-seated gravitational slope deformation (DSGSD) and slow-moving landslides in the southern Tien Shan Mountains: New insights from InSAR, tectonic and geomorphic analysis. *Earth Surf. Process. Landf.* **2019**, *44*, 2333–2348. [CrossRef]
32. Agnesi, V.; Conoscenti, C.; Di Maggio, C.; Rotigliano, E. Geomorphology of the Capo San Vito Peninsula (NW Sicily): An Example of Tectonically and Climatically Controlled Landscape. In *Landscapes and Landforms of Italy*; Soldati, M., Marchetti, M., Eds.; World Geomorphological Landscapes; Springer: Cham, Switzerland, 2017; pp. 455–465, ISBN 978-3-319-26192-8.
33. Agnesi, V.; Macaluso, T.; Monteleone, S.; Pipitone, G. Espansioni Laterali (Lateral Spreads) Nalla Sicilia Occidentale. *Geol. Appl. Idrogeol.* **1978**, *13*, 319–326.
34. Agnesi, V.; Pingue, F.; Rotigliano, E.; Di Maggio, C.; Luzio, D.; Tammaro, U. Realizzazione Di Una Rete Di Monitoraggio Geodetico Della Frana Di Scopello (Sicilia Nord-Occidentale). *Mem. Soc. Geol. Ital.* **2006**, *2*, 15–27.

35. Agnesi, V.; Rotigliano, E.; Tammaro, U.; Cappadonia, C.; Conoscenti, C.; Obrizzo, F.; Di Maggio, C.; Luzio, D.; Pingue, F. GPS Monitoring of the Scopello (Sicily, Italy) DGSD Phenomenon: Relationships Between Surficial and Deep-Seated Morphodynamics. In *Engineering Geology for Society and Territory*; Lollino, G., Giordan, D., Crosta, G.B., Corominas, J., Azzam, R., Wasowski, J., Sciarra, N., Eds.; Springer: Cham, Switzerland, 2015; Volume 2, pp. 1321–1325, ISBN 978-3-319-09056-6.
36. Di Maggio, C.; Madonia, G.; Vattano, M. Deep-Seated Gravitational Slope Deformations in Western Sicily: Controlling Factors, Triggering Mechanisms, and Morphoevolutionary Models. *Geomorphology* **2014**, *208*, 173–189. [CrossRef]
37. Di Maggio, C.; Madonia, G.; Vattano, M.; Agnesi, V.; Monteleone, S. Geomorphological Evolution of Western Sicily, Italy. *Geol. Carpathica* **2017**, *68*, 80–93. [CrossRef]
38. Pappalardo, G.; Mineo, S.; Cappadonia, C.; Di Martire, D.; Calcaterra, D.; Tammaro, U.; Agnesi, V. A Combined Gnss-Dinsar-Irt Study for the Characterization of a Deep-Seated Gravitational Slope Deformation. *Ital. J. Eng. Geol. Environ.* **2021**, *1*, 151–162. [CrossRef]
39. Costantini, M.; Ferretti, A.; Minati, F.; Falco, S.; Trillo, F.; Colombo, D.; Novali, F.; Malvarosa, F.; Mammone, C.; Vecchioli, F.; et al. Analysis of Surface Deformations over the Whole Italian Territory by Interferometric Processing of ERS, Envisat and COSMO-SkyMed Radar Data. *Remote Sens. Environ.* **2017**, *202*, 250–275. [CrossRef]
40. Di Martire, D.; Paci, M.; Confuorto, P.; Costabile, S.; Guastaferro, F.; Verta, A.; Calcaterra, D. A Nation-Wide System for Landslide Mapping and Risk Management in Italy: The Second Not-Ordinary Plan of Environmental Remote Sensing. *Int. J. Appl. Earth Obs. Geoinf.* **2017**, *63*, 143–157. [CrossRef]
41. Cappadonia, C.; Confuorto, P.; Sepe, C.; Di Martire, D. Preliminary Results of a Geomorphological and DInSAR Characterization of a Recently Identified Deep-Seated Gravitational Slope Deformation in Sicily (Southern Italy). *Rend. Online Soc. Geol. Ital.* **2019**, *49*, 149–156. [CrossRef]
42. Sulli, A.; Agate, M.; Zizzo, E.; Gasparo Morticelli, M.; Lo Iacono, C. Geo-Hazards of the San Vito Peninsula Offshore (Southwestern Tyrrhenian Sea). *J. Maps* **2021**, *17*, 185–196. [CrossRef]
43. Catalano, R.; Valenti, V.; Albanese, C.; Accaino, F.; Sulli, A.; Tinivella, U.; Gasparo Morticelli, M.; Zanolla, C.; Giustiniani, M. Sicily's Fold–Thrust Belt and Slab Roll-Back: The SI.RI.PRO. Seismic Crustal Transect. *J. Geol. Soc.* **2013**, *170*, 451–464. [CrossRef]
44. Caracausi, A.; Sulli, A. Outgassing of Mantle Volatiles in Compressional Tectonic Regime Away From Volcanism: The Role of Continental Delamination. *Geochem. Geophys. Geosyst.* **2019**, *20*, 2007–2020. [CrossRef]
45. Gugliotta, C.; Gasparo Morticelli, M.; Avellone, G.; Agate, M.; Barchi, M.R.; Albanese, C.; Valenti, V.; Catalano, R. Middle Miocene–Early Pliocene Wedge-Top Basins of NW Sicily (Italy): Constraints for the Tectonic Evolution of a 'Non-Conventional' Thrust Belt, Affected by Transpression. *JGS* **2014**, *171*, 211–226. [CrossRef]
46. Agate, M.; Basilone, L.; Di Maggio, C.; Contino, A.; Pierini, S.; Catalano, R. Quaternary Marine and Continental Unconformity-Bounded Stratigraphic Units of the NW Sicily Coastal Belt. *J. Maps* **2017**, *13*, 425–437. [CrossRef]
47. Catalano, R.; Avellone, G.; Basilone, L.; Contino, A.; Agate, M. *Carta Geologica d'Italia Alla Scala 1:50.000 e Note Illustrative Dei Fogli 609–596 Termini Imerese—Capo Plaia*; ISPRA: Rome, Italy, 2011.
48. Sacco, P.; Battagliere, M.L.; Coletta, A. COSMO-SkyMed Mission Status: Results, Lessons Learnt and Evolutions. In Proceedings of the 2015 IEEE International Geoscience and Remote Sensing Symposium (IGARSS), Milan, Italy, 26–31 July 2015; IEEE: New York, NY, USA; pp. 207–210.
49. Costantini, M.; Falco, S.; Malvarosa, F.; Minati, F. A New Method for Identification and Analysis of Persistent Scatterers in Series of SAR Images. In Proceedings of the IGARSS 2008—2008 IEEE International Geoscience and Remote Sensing Symposium, Boston, MA, USA, 6–11 July 2008; IEEE: New York, NY, USA; pp. II-449–II-452.
50. Mikola, R.G. ADONIS: A Free Finite Element Analysis Software with an Interactive Graphical User Interface for Geoengineers. In Proceedings of the GeoOttawa2017 Conference, San Francisco, CA, USA, 1–4 October 2017.
51. Forgia, V.; Sineo, L. Within the Symbolic World of the Prehistoric Hunters: A GIS-Based and 3D Model Analysis of Sites with Complexes of Linear Incisions in Western Sicily. *Digit. Appl. Archaeol. Cult. Herit.* **2021**, *20*, e00175. [CrossRef]
52. Martinello, C.; Mercurio, C.; Cappadonia, C.; Bellomo, V.; Conte, A.; Mineo, G.; Di Frisco, G.; Azzara, G.; Bufalini, M.; Materazzi, M.; et al. Using Public Landslide Inventories for Landslide Susceptibility Assessment at the Basin Scale: Application to the Torto River Basin (Central-Northern Sicily, Italy). *Appl. Sci.* **2023**, *13*, 9449. [CrossRef]
53. Abate, S.; Albanese, C.; Angelino, A.; Balasco, M.; Bambina, B.; Bellani, S.; Bertini, G.; Botteghi, S.; Bruno, P.P.; Caielli, G.; et al. VIGOR: Sviluppo Geotermico Nella Regione Sicilia—Studi Di Fattibilità a Mazara Del Vallo e Termini Imerese, Valutazione Geotermica Con Geofisica Elitrasportata. In *Progetto VIGOR—Valutazione Del Potenziale Geotermico Delle Regioni Della Convergenza, POI Energie Rinnovabili e Risparmio Energetico 2007–2013*; CNR-IGG 2014; IRIS: London, UK, 2015.
54. Pasuto, A.; Soldati, M. 7.25 Lateral Spreading. In *Treatise on Geomorphology*; Elsevier: Amsterdam, The Netherlands, 2013; pp. 239–248, ISBN 978-0-08-088522-3.
55. Di Martire, D.; Novellino, A.; Ramondini, M.; Calcaterra, D. A-differential synthetic aperture radar interferometry analysis of a deep seated gravitational slope deformation occurring at Bisaccia (Italy). *Sci. Total Environ.* **2016**, *550*, 556–573. [CrossRef]
56. Fenelli, G.B.; Picarelli, L.; Silvestri, F. Deformation process of a hill shaken by the Irpinia earthquake in 1980. In Proceedings of the French-Italian Conference on Slope Stability in Seismic Areas, Imperia, Italy, 14–15 May 1992; pp. 47–62.
57. Crosetto, M.; Solari, L.; Mróz, M.; Balasis-Levinsen, J.; Casagli, N.; Frei, M.; Oyen, A.; Moldestad, D.A.; Bateson, L.; Guerrieri, L.; et al. The Evolution of Wide-Area DInSAR: From Regional and National Services to the European Ground Motion Service. *Remote Sens.* **2020**, *12*, 2043. [CrossRef]

58. Glueer, F.; Loew, S.; Manconi, A.; Aaron, J. From Toppling to Sliding: Progressive Evolution of the Moosfluh Landslide, Switzerland. *JGR Earth Surf.* **2019**, *124*, 2899–2919. [CrossRef]
59. Agliardi, F.; Scuderi, M.M.; Fusi, N.; Collettini, C. Slow-to-Fast Transition of Giant Creeping Rockslides Modulated by Undrained Loading in Basal Shear Zones. *Nat. Commun.* **2020**, *11*, 1352. [CrossRef]
60. Peduto, D.; Ferlisi, S.; Nicodemo, G.; Reale, D.; Pisciotta, G.; Gullà, G. Empirical Fragility and Vulnerability Curves for Buildings Exposed to Slow-Moving Landslides at Medium and Large Scales. *Landslides* **2017**, *14*, 1993–2007. [CrossRef]
61. Petley, D.N.; Allison, R.J. The Mechanics of Deep-seated Landslides. *Earth Surf. Process. Landf.* **1997**, *22*, 747–758. [CrossRef]